HHS Public Access

Author manuscript

Mater Sci Eng C Mater Biol Appl. Author manuscript; available in PMC 2018 October 01.

Published in final edited form as:

Mater Sci Eng C Mater Biol Appl. 2017 October 01; 79: 270–279. doi:10.1016/j.msec.2017.05.052.

The Bone Building Blues: Self-hardening copper-doped calcium phosphate cement and its *in vitro* assessment against mammalian cells and bacteria

Julietta V. Rau[1,*], **Victoria M. Wu**[2], **Valerio Graziani**[1], **Inna V. Fadeeva**[3], **Alexander S. Fomin**[3], **Marco Fosca**[1], and **Vuk Uskoković**[2,*]

[1]Istituto di Struttura della Materia, Consiglio Nazionale delle Ricerche (ISM-CNR), Via del Fosso del Cavaliere, 100–00133 Rome, Italy

[2]Department of Biomedical and Pharmaceutical Sciences, Center for Targeted Drug Delivery, Chapman University, Irvine, CA 92618-1908, USA

[3]AA Baikov Institute of Metallurgy and Materials Science, Russian Academy of Sciences, Leninsky prospect 49, 119991 Moscow, Russia

Abstract

A blue calcium phosphate cement with optimal self-hardening properties was synthesized by doping whitlockite (β-TCP) with copper ions. The mechanism and the kinetics of the cement solidification process were studied using energy dispersive X-ray diffraction and it was found out that hardening was accompanied by the phase transition from TCP to brushite. Reduced lattice parameters in all crystallographic directions resulting from the rather low (1:180) substitution rate of copper for calcium was consistent with the higher ionic radius of the latter. The lower cationic hydration resulting from the partial Ca→Cu substitution facilitated the release of constitutive hydroxyls and lowered the energy of formation of TCP from the apatite precursor at elevated temperatures. Addition of copper thus effectively inhibited the formation of apatite as the secondary phase. The copper-doped cement exhibited an antibacterial effect, though exclusively against gram-negative bacteria, including *E. coli*, *P. aeruginosa* and *S. enteritidis*. This antibacterial effect was due to copper ions, as demonstrated by an almost negligible antibacterial effect of the pure, copper-free cement. Also, the antibacterial activity of the copper-containing cement was significantly higher than that of its precursor powder. Since there was no significant difference between the kinetics of the release of copper from the precursor TCP powder and from the final, brushite phase of the hardened cement, this has suggested that the antibacterial effect was not solely due to copper ions, but due to the synergy between cationic copper and a particular phase and aggregation state of calcium phosphate. Though inhibitory to bacteria, the copper-doped cement increased the viability of human glial E297 cells, murine osteoblastic K7M2 cells and especially human primary lung fibroblasts. That this effect was also due to copper ions was

[*]Corresponding authors: giulietta.rau@ism.cnr.it and uskokovi@chapman.edu.

evidenced by the null effect on viability increase exhibited by the copper-free cements. The difference in the mechanism of protection of dehydratases in prokaryotes and eukaryotes was used as a rationale for explaining the hereby evidenced selectivity in biological response. It presents the basis for the consideration of copper as a dually effective ion when synergized with calcium phosphates: toxic for bacteria and beneficial for the healthy cells.

Keywords

copper-doped calcium phosphate cement; brushite; hardening behavior; solidification kinetics; calcium ion substitution; *in vitro* properties; eukaryotic cells; bacteria

1. Introduction

The clinical necessity of bone grafts has been growing recently as a direct corollary of the increase of the average life expectancy and the increase of the incidence of diseases of the skeletal system [1]. Due to the similar chemical composition and properties to the natural bone mineral, Tricalcium Phosphate (TCP) is widely used as a common biomaterial for bone substitutes, implant coatings, dental materials, biomedical cements, composite components and for other applications [2]. It has an advantage over hydroxyapatite, the synthetic version of the bone mineral, in its higher bioresorbability rate [3], due to which it is often mixed in with apatite to yield biphasic bone fillers with resorption rates matching better the new bone ingrowth rates than apatite alone [4]. However, it is well-known that bacteria can be adsorbed and replicated on the TCP surface [5], inducing serious implant-related infections. One way of coping with this issue is to administer antibiotics postoperatively, either systemically or locally, the latter of which is thanks to the ability of calcium phosphate cements to bind antibiotics and release them sustainably [6]. The use of antibiotics is, however, costly and is linked with the global problem of rising immunity of pathogens to traditional antibiotic therapies [7]. The use of antibacterial cations as substitutes for calcium ions in the TCP structure, e.g., Ag^{+}, Cu^{2+} and Zn^{2+}, has been proposed as a way to amend these two major downsides of the use of traditional antibiotics [1, 8–11]. Copper is an essential redox metallic ion figuring as a cofactor for intracellular enzymes involved in a number of physiological processes, ranging from signal transduction to energy generation to oxygen transport to cell metabolism to blood clotting [12]. Its deficiency or disrupted homeostasis are directly linked with disease states [13]. As far as its effect on bone health is concerned, its deficiency has decreased bone strength [14], while its use as a diet supplement reduced bone loss in menopausal women [15,16]. Alongside having a role in mineralization, it is a cofactor for lysyl oxidase, an enzyme crosslinking collagen fibers and increasing the integrity of the bone connective tissue [17]. In this study, it was investigated as a dopant in a self-hardening TCP cement.

In addition to antibacterial properties, an ideal bone substitute should also possess an intrinsic potential to foster the bone growth. To fulfill this purpose, growth factors are often used as supplements in bone cements. However, they are associated with high cost [18] and with a range of undesired side effects [19–22], the reason for which ionic additives are often considered as viable alternatives to their use: not only are they considerably less expensive,

but there is also a markedly lesser chance that their delivery would cause adverse effects. The third potentially positive effect achievable with the addition of copper ions is an increased solubility and resorption rate of TCP. Namely, TCP is widely used as material for bone replacement (Poresorbs-TCP®, Easy Graft®, ChronOS®), but rather low biodegradation rate of sintered, nonporous TCP limits its applications. The isomorphic substitution of Ca^{2+} ions with Cu^{2+} ions may lead to distortion of the TCP lattice because the ionic radius of copper ions (0.73 Å) is significantly lesser than that of calcium ions (1 Å) [23].

To the best of our knowledge, this is the first report on a copper-doped TCP cement, a self-hardening bone filler distinctly blue in color. The aim of the reported investigation was to study: (a) the method of producing a copper-doped calcium phosphate cement; (b) its self-hardening mechanism and kinetics; and (c) its antibacterial and cytophilic characteristics.

2. Materials and Methods

Pure TCP and Cu^{2+}-substituted TCP powders were obtained using a precipitation technique [24] according to the following reaction:

$$(3- x)Ca(NO_3)_2+xCu(NO_3)_2+2(NH_4)_2HPO_4 \rightarrow Ca_{3- x}Cu_x(PO_4)_2, \quad (1)$$

where x= 0 or 0.1.

Synthesis procedure was as follows: the 0.5 mol/L solution of $Ca(NO_3)_2$ were mixed with a calculated amount of $Cu(NO_3)_2$ solution; then, $(NH_4)_2HPO_4$ solution was added dropwise with the rate of 20 mL/min (1). The pH level was kept at 6.5–6.9 by the dropwise addition of ammonia solution. After 30 min, the precipitate was filtered, washed with distilled water and dried at 80°C. The precipitate was calcined at 900°C in order to remove the traces of NH_4NO_3 and to form the whitlockite structure. Then, the elemental (atomic emission spectrometry with inductively coupled plasma “Ultima-2”) and the XRD (Shimadzu 6000) analyses were performed.

Coherent scattering area and lattice parameters were calculated using crystallographic computing system for standard and modulated structures Jana 2006. For this purpose, the XRD investigations were performed on the Rigaku D/Max-2500 diffractometer with a rotating anode (Japan). The study was carried out in the reflection mode (geometry Bragg-Brentano geometry) using CuKα radiation (average wavelength λ=1.54183 Å). The parameters of the generator: accelerating voltage is 50 kV, tube current of 250 mA. The range of angles 2Theta = 2–60, step 0.02. Quartz cells were employed. Qualitative analysis of the obtained radiographs was performed using the program package WinXPOW and the database ICDD PDF -2.

Infrared spectra of the powders were examined in the KBr pellet and on the Nikolet Avatar 330 FT-IR spectrometer in the 400–4000 cm^{-1} wavenumber range.

The CuTCP cement was obtained by a solid-solid mixing of the CuTCP powder with Monocalcium Phosphate Monohydrate (MCPM) and Carbonated Hydroxyapatite (CHA) (mass proportion: 1:0.764:0.091) and, finally, with a solution of citric acid (0.45M). The powder-to-liquid ratio was 4.08 g/mL and the cement set within a minute. The product of the setting reaction is Dicalcium Phosphate Dihydrate (DCPD, brushite):

$$Ca_3(PO_4)_2 + Ca(H_2PO_4)_2 \cdot H_2O + 7H_2O \rightarrow 4CaHPO_4 \cdot 2H_2O \quad (2)$$

A time-resolved XRD characterization of the setting cement was carried out by means of an EDXRD home-made instrumentation [25–28], equipped with a W radiogen tube operating at 50kV, 30 mA, 200 μm wide apertures and θ°=5°. After manual mixing with a putty knife, a small quantity of the cement was quickly transferred (within one minute) to the optical centre of the diffractometer, on a low scattering glass sample holder.

The release of copper ions from the CuTCP powder and its cement were investigated through immersion of 10 mg of the material in 1 mL distilled water and periodically sampling out 25 μL aliquots. The aliquots were mixed with 25 μL of concentrated ammonia as the complexing agent in 96 well plates and measured for absorbance at λ=600 nm on a UV/Vis spectrophotometer (Nanodrop 2000, Thermo Scientific). The absorbance values were converted to concentration units with the use of a calibration curve constructed using a copper salt solution of known concentration.

Biological experiments on eukaryotic cells involved K7M2 murine osteosarcoma cells, U87 and E297 human glioblastoma cells, and human primary lung fibroblasts. K7M2 and U87 cell lines were purchased from ATCC, whereas E297 cell line is the courtesy of H. H. Engelhard (University of Illinois, Chicago) and the primary lung fibroblasts of R. Ostrom (Chapman University). Cells obtained from different sources were cultured separately, in standard 24 well plates (Corning), at 37°C and 5% CO_2 in MEM-α (Gibco) media supplemented with 10 % FBS and 1 % antibiotic-antimycotic (Gibco) to prevent bacterial and fungal contamination. After 24 – 36 h of culture, 5 mg of hardened cement was suspended in 1 mL of the growth medium and added to the confluent cells. After the particles were incubated with the cells for 24 h, the cells were tested for viability. MTT (3-(4,5-Dimethylthiazol-2-yl)-2,5-Diphenyltetrazolium Bromide) solution was prepared and run according to the manufacturer's instructions (VybrantR MTT Cell Proliferation Assay Kit V-13154) and absorbance was measured at 540 nm using a microplate reader (FLUOstar Omega, BMG LABTECH). All the samples for this assay were analyzed in quadruplicates.

Hardened TCP and CuTCP cements were tested for their antibacterial activity against *Escherichia coli, Staphylococcus aureus, Salmonella enteritidis,* and *Pseudomonas aeruginosa* using the agar diffusion and liquid inoculation assays. Ten mg of the cement were placed as a paste onto a bacterium-infused nutrient agar plate with the spot radius of 1 cm. The plates were then allowed to incubate for 24 h at 37 °C. The zone of inhibition was used to visually gauge the antibacterial activity of the cements. In addition, a 1 mm scratch was made with a p200 pipette tip across the surface of the agar plate at different distances from the center of the plate. The pipette tip containing the scraped bacteria was then

immersed in 20 μL of a nutrient broth and the optical density at 600 nm was measured on a UV/Vis spectrophotometer (Nanodrop2000, Thermo Scientific). All the samples for this assay were analyzed in triplicates. In the liquid inoculation test, a single colony of *S. aureus* cultured on a blood agar plate over a period of 24 h was stabbed with a pipette tip, placed in 5 mL of brain heart infusion broth (*Sigma Life Sciences*) containing 10 mg/mL CuTCP, and incubated overnight at 37 °C and 170 rpm. The same procedure was repeated for other bacteria. All the samples for this assay were analyzed in triplicates.

3. Results and Discussion

The copper content in the Cu^{2+}-substituted TCP powder (CuTCP) was 0.30 wt.% according to the results of the elemental analysis. The discrepancy between this value and the value calculated from the stoichiometry of the precursors (2.05 wt%) is explained by the fact that, while a part of Cu^{2+} ions substituted Ca^{2+} in the TCP structure, a large part of Cu^{2+} formed water-soluble amminocomplexes with NH_4^+ ions from the reaction mixture and was washed away in the filtrate. The resulting stoichiometry of CuTCP could be represented as $Ca_{2.984}Cu_{0.016}(PO_4)_2$, meaning that only one out of ~ 180 Ca atoms was replaced by Cu. Such a substitution rate is lower than that usually observed in hydroxyapatite also because of the lesser susceptibility to vacancies and to lattice strain in TCP.

In Fig.1, the results of the XRD analysis are shown. All the peaks in the two diffractograms originate from whitlockite (β-TCP), the main phase after calcination at 900°C. A slight shift of all the diffraction peaks to higher 2θ supports the hypothesis of the Ca→Cu substitution. Namely, a shift of reflections to higher 2θ correlates with smaller interplanar distances and the smaller unit cell volume, which is expected considering the smaller atomic size of Cu than that of Ca. The shifts for the main Bragg reflections are reported in Table 1 as $\Delta_{2\theta}$.

The Rietveld refinement of the diffractograms confirmed the substitution of Ca^{2+} ions with Cu^{2+} ions in the TCP crystal structure. The cell parameters of pure TCP are a=b=10.429 Å and c=37.380 Å, while those of Cu-substituted TCP are a=b=10.413 Å and c=37.335 Å. The decrease of cell parameters values is an additional evidence of the substitution of Ca^{2+} ions (with a greater ionic radius) with Cu^{2+} ions (with a smaller ionic radius).

In both powder samples, TCP and CuTCP, a small amount of the apatite phase was detected (the most intense (211) reflection (100% RI), PDF card number #090432) [29]). The partial substitution of Ca^{2+} with Cu^{2+} in the TCP structure did not affect the crystallinity, as no broadening of the CuTCP peaks was detected.

The coherent scattering area (CSA) of TCP and CuTCP powders was measured, and the results are presented in Table 2. The lower CSA value for CuTCP suggests that copper ions substitute calcium ions in the TCP crystal lattice.

Infrared spectra (Fig. 2) confirm whitlockite as the main phase, in agreement with the XRD data. The doublet at 560–610 cm^{-1} is attributed to the triply degenerated bending mode, ν_4, of the phosphate group and is typical for the whitlockite structure. The triplet in the 420–480 cm^{-1} range originates from the doubly degenerate bending mode, ν_2, of the phosphate group. Absorption bands at 962 and 875 cm^{-1} are different modes of the ν_1 symmetric

stretching vibration of the phosphate group. The asymmetric ν_3 stretch is detected as the doublet at 1020 and 1120 cm^{-1}. Nitrate residues are detected as bands at 820 and 1380 cm^{-1}. The sharp band at 3570 cm^{-1} belongs to the stretch of OH^- groups constituting the minorly present apatite phase. In contrast, the wide band in the 2600–3600 cm^{-1} range originates from adsorbed, non-structural water molecules. It is interesting that the sharp $\nu_1(OH)^-$ stretching vibration at 3570 cm^{-1} was observed in the pure TCP spectrum only, which may indicate the presence of apatite phase [30]. The bending mode of OH^- vibration at 630 cm^{-1} is also more intense in TCP powders not doped with Cu (CuTCP band at 1640 cm^{-1} derives from adsorbed water [31]). Since both as-precipitated powders, with and without Cu, contained apatite, the ability of Cu to reduce the thermal stability of the apatite phase and promote the transition to TCP phase must be exerted during the annealing stage. Compared to Ca^{2+} ions occupying the far, strongly hydrated end of the Hofmeister series and having an apparent affinity for OH^- ions, the thermal stability of copper hydroxide is significantly lower, e.g. it decomposes into an oxide already at 80 °C, compared to 580 °C for calcium hydroxide. The lower cationic hydration resulting from the partial $Ca^{2+} \rightarrow Cu^{2+}$ substitution is assumed to facilitate the release of the constitutive hydroxyls and, thus, lower the energy of formation of TCP from the apatite precursor at elevated temperatures. The same effect may explain another pronounced difference between the IR spectra of TCP and CuTCP, namely the absence of the most intense carbonate band, the asymmetric ν_3 stretch doublet centered at 1430 cm^{-1}, in the former and its presence in the latter. Another carbonate band at 870 cm^{-1} cannot be distinguished in the spectra since it is covered by the $\nu_1(PO_4)^{3-}$ stretching vibration at 875 cm^{-1}. Unlike calcium hydroxide, copper hydroxide spontaneously transforms to basic copper carbonate under ambient conditions, illustrating the affinity of Cu^{2+} for CO_3^{2-} ions. Even though carbonates typically fully evaporate from calcium phosphates by the time the sample reaches 950 °C [31], in this case carbonates were retained in the material owing to the presence of Cu^{2+}. In its absence, carbonates disappear from the material following the annealing at 900 °C. Hence, no carbonate group bands were detected in the IR spectrum of TCP, confirming the low propensity for $PO_4^{3-} \rightarrow CO_3^{2-}$ substitution in TCP annealed at temperatures exceeding 800 °C [32], contrasting the high propensity for such a transition in apatite [33]. It is possible that the contracted lattice resulting from the cationic exchange of larger Ca^{2+} ions for smaller Cu^{2+} presents an additional factor favoring the complementary substitution of similarly larger phosphates for smaller carbonates.

CuTCP based bone cement was investigated using EDXRD for 100 h after the mixing with continuous acquisitions. The acquisition times of the spectra were: 60 s for the first ten spectra (till the 10^{th} min from the mixing), 120 s for the subsequent ten spectra (till the 30^{th} min from the mixing), 5 min for the subsequent six spectra (1^{st} h reached), 10 min for the next twelve spectra (3^{rd} h reached), 15 min for the successive three-hundred-eighty-eight spectra (100^{th} h reached).

In Fig. 3, the initial (60 s) and final spectra (100 h) of the CuTCP cement after the mixing are shown. The pattern at 60 s is characterized by the presence of an amorphous component of the system (corresponding mainly to the liquid phase with the contribution of the non-crystallized products of the reaction). In these conditions, only a few peaks can be well distinguished: brushite (041), (2̲21), (1̲12) and (2̲20)&(2̲02), respectively at q=2.03, 2.17,

2.22, 2.37 $Å^{-1}$ (card number: #090077); Cu_4O_3 (202)&(004) and (220), respectively at q=2.53, 3.07 $Å^{-1}$ (card number: #831665); $Ca_3(PO_4)_2$ (205), (015), (110), (024), respectively at q=3.23, 2.17, 2.39 (shoulder), 3.07 $Å^{-1}$ (card number: #320176) [29]. In the final pattern, registered after 100 h, the main phase, as expected, can be reliably assigned to brushite, as testified by the presence of its the most intense diffraction peaks.

The transformation of TCP into brushite, recognizable already in the first 60 s after mixing, demonstrates a rapid progression of the reaction. The presence of Cu_4O_3, in which copper shows different oxidation states (+1 and +2), suggests a complex reaction path during the hardening process. The overall profile of the last spectrum is very different from the initial one, especially in the range of 2.5÷3.5 $Å^{-1}$. The amorphous phase diminishes during the hardening process, while the new highly crystalline peaks of brushite appear ((151); (2̲42); (3̲11)&(1̲52) and (241)&(062), respectively, at q=2.86, 2.96, 3.01, 3.46 $Å^{-1}$) [29]. The presence of the sharp peaks in the final diffractogram demonstrates that the final brushite phase is crystalline. The average crystallite size was estimated from Scherrer's equation for three of the main peaks: 92±6 A for (041), 110±2 A for (241)&(062) and 125.5±0.5 Å for (2̲42). Considering, however, that the first and the second values are obtained from the mixed peaks containing different contributions, leading to an enlargement of the FWHM (Full Width Half Maximum) and then to a reduction of the grain size, the most reliable value is that of 125.5±0.5 Å, obtained from the non-mixed (2̲42) peak.

An interesting observation is given by the (041) peak, the most intense in the q range analyzed: while the first spectrum shows a tight, sharp peak centred at q=2.03 $Å^{-1}$ (black line in Fig. 3), the final spectrum at the same position displays a large overlap of at least two peaks. Since the contribution of the brushite at the theoretical value is clearly recognizable in the final spectrum (dashed dot line in Fig. 3), we can hypothesize that: 1) at the early stage of brushite crystallization a certain process occurs resulting in a modified structure; 2) this process ceases at a certain time and the normal crystallization of brushite begins, resulting in the overlap of two peaks belonging to slightly different brushite phases. As a further investigation, in Table 3, the observed values of the scattering parameter q($Å^{-1}$) for six brushite peaks are compared with the theoretical values; for the coupled peaks, the observed value is referred to as the resulting sum peak found in the spectrum, while the expected value is referred to as the theoretical one nearer to the observed value.

Only for the last two couples of peaks are the differences not significant, taking into account the EDXRD resolution, while the repeated differences for the other couples of values could be interpreted as shifts. This suggests that the brushite phase formed in this system has crystallographic features different from that of non-substituted brushite. This could be related to the effect of copper ions substituting the calcium ones in the brushite structure so long as they are available in the system. In analogy with the higher solubility of calcium-deficient apatites than that of stoichiometric apatite [34], it is expected that such a cationic substitution in the brushite structure will lead to stresses and distortions in the lattice, resulting in a decrease of crystallinity and, consequently, in the increase of solubility. Brushite is more soluble than TCP but with *in vivo* environment forms an apatite-based surface of reaction that makes the implant material non-resorbable with the time. Such a

cationic substitution, enhancing the solubility of the brushite and preventing the formation of the apatite, should be considered an improvement of the performance of the material.

In Fig. 4, the overall evolution of the system is presented by means of a 3D representation of the diffraction pattern time evolution. In this 3D diffraction map, it is possible to observe the presence of intermediate phases and the related timepoints at which they appear and disappear, confirming the complexity of the reaction path. In the map, at least two significant variations of the amorphous phase contribution are evident, producing discontinuities in the trend of the pattern evolution: the first one occurs at the end of the 7^{th} min, the second one at the end of the 12^{th} min. Over the first discontinuity, important modifications occur, with the disappearing of the peaks at q=1.93 $Å^{-1}$; q=2.76 $Å^{-1}$; q=3.14 $Å^{-1}$; q=3.22 $Å^{-1}$; q=3.41 $Å^{-1}$; q=3.77 $Å^{-1}$; q=3.94 $Å^{-1}$; q=4.25 $Å^{-1}$.

Over the second discontinuity, other important modifications take place:

- **i.** new peaks appear at: q=2.03 $Å^{-1}$; q=2.18 $Å^{-1}$; q=2.39 $Å^{-1}$; q=4.39 $Å^{-1}$
- **ii.** peaks disappear at: q=2.24 $Å^{-1}$; q=3.85 $Å^{-1}$; q=4.03 $Å^{-1}$
- **iii.** peaks show the trend to disappear at: q=2.12 $Å^{-1}$; q=2.51 $Å^{-1}$; q=2.92 $Å^{-1}$; q=3.17 $Å^{-1}$; q=3.51 $Å^{-1}$
- **iv.** peaks disappear but the new ones appear in the spectrum corresponding to the 14^{th} min exhibiting several shifts: the peak at q=3.68 $Å^{-1}$, q=3.31–3.34 $Å^{-1}$ (couple of peaks) and q=3.01 $Å^{-1}$ shift respectively to q=3.72 $Å^{-1}$, q=3.29 $Å^{-1}$ and q=3.04 $Å^{-1}$.

The compositional stabilization of the system is reached after 60 min, although some variations in the diffracted intensity are still present, demonstrating the persistence of a secondary crystallization. This behaviour of the cement was further quantitatively investigated by means of kinetic curves, related to three main brushite peaks registered in the final spectrum: (041), ($\bar{2}$42) and (241)&(062). The time evolution of their diffracted intensity is shown in Fig. 5. While the ($\bar{2}$42) and (241)&(062) peak profiles are analogous and follow the sigmoidal trend, the (041) peak has a more complex intensity variation with at least two maxima at 2.5 h and 14 h. Considering all three curves, the cement becomes definitely stable after 40 h of the hardening time. No significant variation was found for the crystallite sizes and for the lattice parameters of the three peaks evolving through time.

Results of the agar diffusion tests carried out on the Cu-TCP cement immediately after the initiation of the hardening process are shown in Fig. 6. The cement exhibited an antibacterial effect, though exclusively against the gram-negative bacteria: *E. coli*, *P. aeruginosa* and *S. enteritidis*. Correspondingly, the bacterial concentrations exhibit a gradual drop moving from the maximally bacterially populated edge of the dish to the cement positioned in its center (Fig. 6b–d). In contrast, the cement appears to increase the proliferation of gram-positive *S. aureus*, as shown in Fig.6a. Thus, the concentration of this bacterium displayed a significant increase in the immediate vicinity of the cement compared to rest of the dish (Fig. 6a). Though effective in inhibiting gram-negative bacteria under the solid invasion conditions, the cements were not effective at suppressing the bacterial growth in liquid broth conditions under the same concentrations of the solid phase and of the inoculate (Fig.S1). This has

implied that the bacterial inhibition is more probable to take place with Cu-TCP in the solid form than in the dispersed form in a liquid phase. This is natural in view of the fact that this type of material is intended for the application as a resorbable bone tissue substitute and not as a colloidal antibacterial agent.

Results of the comparison of the antibacterial activity of CuTCP cement in the agar diffusion assay against the activities of the precursor CuTCP and TCP powders and of the Cu-free TCP cement are shown in Figs.7–8. The antibacterial activity indicated by the inhibition zone diameters was significantly more pronounced for the CuTCP cement than for any of the other three experimental groups. That the antibacterial effect of CuTCP was due to copper ions and not to any of the CP phases in the cement or the side effects of the transitions between them is demonstrated by an almost negligible antibacterial effect of the pure TCP cement. Thus, as seen from Figs. 7–8, negligibly minor inhibition zone were detected around the TCP cement and none around the corresponding TCP precursor powder, contrasting the prominent inhibition zones around CuTCP cement. Interestingly, also, the antibacterial activity of CuTCP cement was significantly higher than that of the CuTCP precursor powder. Thus, whereas the inhibition zone diameters for CuTCP cement ranged from 1.26 to 1.29 to 1.68 cm against *P. aeruginosa*, *S. enteritidis* and *E. coli*, respectively, these diameters were by an order of magnitude lower for the corresponding CuTCP powder, ranging from 0 to 0.22 to 0.16 cm for the given bacterial strains. This difference suggests that the phase composition and the microstructure of ion-substituted calcium phosphate can have a decisive effect on the exhibition of activity typifying the given ion. Though the concentration of Cu in the material becomes lowered (~ 3x) following the mixing of the precursor CuTCP powder with the additional calcium phosphate components and with the liquid phase, the resulting antibacterial effect of the copper ion becomes significantly larger.

It was initially thought that copper ions might be released more intensely to the surrounding space from the more soluble brushite phase of the CuTCP cement than from the less soluble TCP phase present in the precursor CuTCP powder, explaining for the greater antibacterial effect of the cement compared to its precursor. However, as seen from Fig. 9, the release of copper ions from the CuTCP powder exceeds that from the cement at all hours but the first one following the immersion in water. That is, when identical amounts of the CuTCP powder and CuTCP cement are compared, the release of copper is obviously more copious from the former. However, when normalized to the amount of the actively releasing, CuTCP component in the cement, no significant difference in the release of copper is observed, both in terms of its order and the amount (Fig. 9). Namely, the slope of the released amount vs. time curve is identical for both CuTCP powder and the cement, whereas after 24 h of the release, which was the duration of the antibacterial assays, there was a negligible difference in the amount of copper released from the CuTCP powder and from the CuTCP component of the cement. The only peculiarity is that the copper release in the first hour was six times greater from the CuTCP cement than from its precursor powder, even though the cement contained ~ 3 times lower amount of CuTCP powder, the remaining components being MCPM, CHA, citrate and water. It is little conceivable that such a more prominent burst release of copper plays a role in increasing the antibiotic efficacy of the material. It is more probable that the antibacterial effect is due to the synergy with the cell/particle contact. Synergistic effects involving citric acid as the sole molecular component of the liquid phase

of the cement may be another factor explaining the higher antibacterial activity of CuTCP cement compared to the CuTCP powder prior to its mixing with the liquid phase. In any case, the fact that the material demonstrating a lower rate of release of copper ions, in this case the CuTCP cement, exhibits a more prominent antibacterial effect indicates that the agent/carrier synergy must be at work.

Cu^{2+}-substituted hydroxyapatite nanoparticles previously demonstrated an antibacterial activity against *E. coli* [9]. The antibacterial effect was expected to be due to the leaching of Cu^{2+} ions, which leads to the lysis of the bacteria cell wall. The toxic effect against *E. coli* is thought to be the result of the displacement of iron from exposed, not buried, iron-sulfur clusters in sopropylmalate dehydratase, fumarase A, 6-phosphogluconate dehydratase, dihydroxy-acid dehydratase, isopropylmalate isomerase and other iron-sulfur enzymes of the common branched-chain and the leucine-specific branch pathway [35]. Generation of reactive oxygen species, the loss of cytoplasmic membrane integrity, inhibited respiration and degradation of DNA all present upstream and downstream outcomes of these disruptions at the molecular level [36,37]. In addition, in analogy with the effect known to apply for iron, copper may react with endogenous hydrogen peroxide and yield mutagenic hydroxyl radicals that induce lethality in bacteria [38,39]. Whereas dehydratases as enzymes sensitive and damageable by the presence of copper are localized deep inside the cytoplasm and copper-containing enzymes are found in the periplasm of *E. coli* and other prokaryotes, eukaryotes do not protect dehydratases by compartmentalization, but by chelation, meaning that the two types of proteins colocalize and engage chaperones in direct delivery of copper to copper-containing proteins. This may explain why bacteria are more affected by the delivery of copper than the eukaryotic cells and may present the basis for the consideration of copper as a selective ion in regenerative bone therapies: toxic for bacteria and beneficial for the healthy cells.

Scaffolds loaded with Cu^{2+} improved not only proliferation and cellular activity of osteoblasts [40] but also *in vivo* vascularization [41,42] while the effect of copper releasing from biomaterials has not been extensively studied, as well as the effect on surrounding living tissues, with respect to the toxicity limit for the cellular copper uptake. To complement the agar diffusion and liquid broth assays, CuTCP cements were then analyzed for cell viability against multiple cell lines. As seen in Fig. 10a, an intense proliferative effect of hardened CuTCP cements was verified on bone cells (K7M2) as well as on patient glial cell line (E297), as opposed to the standard glial cell line (U87).

Interestingly, the precursor CuTCP powder exhibited the opposite effect, hindering the natural proliferation of K7M2 and E297 cells. One possibility is that, as insinuated by the aforementioned antibacterial testing results too, this effect may be due to the synergy between the copper ions and the viscous brushite component comprising the hardened product. The greater release of copper ions directly available to the cells when brought into contact with brushite particles, theoretically more soluble and resorbable than TCP, would have a directly proliferative effect on cells. The osteogenic effect of copper ions delivered either individually [43] or using CP cement [40], bioactive glass [44] or a titanium implant [45] as a carrier has been noticed earlier, but the precise mechanism remains unknown. A dose-dependent analysis of the effect of the material on two fundamentally different types of

human cells – U87 glioblastoma cells and primary lung fibroblasts – demonstrated a proliferative effect exerted on the healthy cells and a reduction in viability of the malign U87 cells (Fig. 10b). A multifold increase in cell viability was observed in healthy fibroblasts following the treatment with the precursor CuTCP powder in the 1 – 2.5 mg/ml dose range, as opposed to a decrease in the viability of U87 cells in the same dose range (Fig. 10b), indicating a selective response of potential therapeutic benefit in prophylaxis of tumorogenesis following the surgical injection of the cement into the body. The complexity of the effect of the cement on cells is illustrated by the diametrically opposite effect it had on two lines of an identical type of cells and derived from the same species: U87 and E297. This complexity agrees with the oft-observed opposite, inhibitory effect of copper on osteoblasts [46,47] with the prevalence of one effect over the other greatly depending on the ionic concentration range and on the presence of absence of synergistically acting species. The combination of an inhibitory effect against gram-negative bacteria and the proliferative effect on osteoblastic K7M2 cells and primary lung fibroblasts is promising in the quest for a bone substitute capable of performing a dual role: preventing and/or inhibiting bacterial growth, while promoting the new bone formation. This is especially so because an increase in the bioactivity of a biomaterial surface usually entails an increase in the biofilm formation propensity too [48]. Still, it is possible that to expand the scope of activity of the cements reported here to gram-positive bacteria, which are causative of the great majority of the clinical cases of bone infection [49], co-delivery of a complementary antibacterial cation is needed. It must also be added that the assays performed here, albeit showing harmlessness to human cells, do not predict the effects that copper will have on organs distant from the site of action and involved in metabolic clearance, such as kidneys or liver. The content of copper in the cement is very low and it would take a daily dissolution of more than 3.33 g of the cement to reach the tolerable upper intake level of copper (10 mg), meaning that the size of the bone defect filler will eventually need to be adjusted to minimize the chances for provoking hepatic damage or other forms of systemic toxicity, which may be minimal for comparatively small or medium sized injection volumes.

5. Conclusions

Two formulations, pure TCP and CuTCP (0.30 wt% Cu^{2+}), were obtained by the precipitation method. According to the XRD and IR analyses, the powders were composed mainly of whitlockite and a small amount of apatite phase. The Ca^{2+} ions substitution by the Cu^{2+} ions in the TCP structure was proved by the following: the presence of shifts between corresponding diffraction peaks in TCP and CuTCP; the decrease of lattice parameters in all crystallographic directions for CuTCP evidenced by the Rietveld refinement; and the different regions of coherent scattering for TCP and CuTCP. The kinetics of the CuTCP cement hardening was investigated using time-resolved EDXRD, and the results showed the transformation of TCP into brushite taking place during the first minutes of the hardening process. A more accurate analysis of the EDXRD results gave a clue about the mechanism of formation of Cu^{2+}-substituted brushite in the cement hardening stage.

The biological effects of the presence of copper in the cement were such that they endowed the cements with a dual response, allowing them to have an inhibitory effect on gram-negative bacteria and proliferative effect on K7M2 bone cells, E297 glial cells and primary

lung fibroblasts. In turn, no effect was observed against U87 glial cells and there was a minor proliferative effect against gram-positive *S. aureus*. That the antibacterial effect was due to copper ions in the cement and not the cement itself was demonstrated by the absence of any antibacterial effect of pure, copper-free cements. The copper-substituted cements also exhibited a significantly higher antibacterial activity against gram-negative bacteria and a more intense proliferative effect on mammalian cells compared to their precursor powders, in spite of the lower concentration of copper in them. In view of the insignificant difference between the kinetics of the release of copper from the precursor TCP powder and from the final, brushite phase of the hardened cement, this was explained by the synergy between cationic copper and a particular phase and aggregation state of the calcium phosphate carrier. This has illustrated that the phase composition and the microstructure of ion-substituted calcium phosphates are bound to have decisive effects on the exhibitions of the activity by the given ion.

Supplementary Material

Refer to Web version on PubMed Central for supplementary material.

Acknowledgments

The Russian Foundation for Basic Research (RFBR grant 15-08-06860-a) and the U.S. National Institutes of Health funding (R00-DE021416) are acknowledged for support.

References

1. Palangkaraya A, Yong J. Population ageing and its implications on aggregate health care demand: empirical evidence from 22 OECD countries. Int J Health Care Finance Econ. 2009; 9:391–402. [PubMed: 19301123]
2. a Dorozhkin SV. Calcium orthophosphates (CaPO4): occurence and properties. Progress in Biomaterials. 2016; 5:9–70. [PubMed: 27471662] b Dorozhkin SV. Calcium orthophosphate-containing biocomposites and hybrid biomaterials for biomedical applications. J Funct Biomater. 2015; 6:708–832. DOI: 10.3390/jfb6030708 [PubMed: 26262645]
3. Gallinetti S, Canal C, Ginebra MP, Ferreira J. Development and Characterization of Biphasic Hydroxyapatite/β-TCP Cements. J Am Ceram Soc. 2014; 97:1065–1073. DOI: 10.1111/jace.12861 [PubMed: 25866411]
4. Hwang JW, Park JS, Lee JS, Jung UW, Kim CS, Cho KS, Lee YK, Choi SH. Comparative evaluation of three calcium phosphate synthetic block bone graft materials for bone regeneration in rabbit calvaria. J Biomed Mater Res B Appl Biomater. 2012; 100:2044–52. DOI: 10.1002/jbm.b.32768 [PubMed: 22865716]
5. Furustrand Tafin U, Betrisey B, Bohner M, Ilchmann T, Trampuz A, Clauss M. Staphylococcal biofilm formation on the surface of three different calcium phosphate bone grafts: a qualitative and quantitative in vivo analysis. J Mater Sci Mater Med. 2015; 26:130.doi: 10.1007/s10856-015-5467-6. [PubMed: 25693675]
6. Uskoković V, Desai TA. Phase Composition Control of Calcium Phosphate Nanoparticles for Tunable Drug Delivery Kinetics and Treatment of Osteomyelitis. I. Preparation and Drug Release. J Biomed Mater Res Part A. 2013; 101:1416–1426. DOI: 10.1002/jbm.a.34426
7. Theuretzbacher U. Accelerating resistance, inadequate antibacterial drug pipelines and international responses. Int J Antimicrob Agents. 2012; 39:295–9. [PubMed: 22341298]
8. Scalny, AV., Rudakov, IA. Bioelements in medicine. Vol. 21. Moscow: Publishing House Onyx; 2004. p. 272

9. Li Y, Ho J, Ooi CP. Antibacterial efficacy and cytotoxicity studies of copper (II) and titanium (IV) substituted hydroxyapatite nanoparticles. Materials Science and Engineering C. 2010; 30:1137–1144.
10. Matsumoto N, Sato K, Yoshida K, et al. Preparation and characterization of β-tricalcium phosphate co-doped with monovalent and divalent antibacterial metal ions. Acta Biomaterialia. 2009; 5:3157–3164. [PubMed: 19435618]
11. Barinov, SM., Fadeeva, IV., Fomin, AS., Petrakova, NV. Method of obtaining porous ceramics of calcium phosphates for the treatment of bone defects. Patent application RF No 2015–112518, priority of 07.04.2015.
12. Kim BE, Nevitt T, Thiele DJ. Mechanisms for copper acquisition, distribution and regulation. Nat Chem Biol. 2008; 4:176–185. [PubMed: 18277979]
13. Madsen E, Gitlin JD. Copper deficiency. Curr Opin Gastroenterol. 2007; 23:187–192. [PubMed: 17268249]
14. Jonas J, Burns J, Abel EW, Cresswell MJ, Strain JJ, Paterson CR. Impaired mechanical strength of bone in experimental copper deficiency. Ann Nutr Metab. 1993; 37:245–252. [PubMed: 8311418]
15. Strause L, Saltman P, Smith KT, Bracker M, Andon MB. Spinal bone loss in postmenopausal women supplemented with calcium and trace minerals. J Nutr. 1994; 124:1060–1064. [PubMed: 8027856]
16. Eaton-Evans J, Mcllrath EM, Jackson WE, McCartney H, Strain JJ. Copper supplementation and the maintenance of bone mineral density in middle-aged women. The Journal of Trace Elements in Experimental Medicine. 1996; 9:87–94.
17. Palacios C. The role of nutrients in bone health, from A to Z. Crit Rev Food Sci Nutr. 2006; 46:621–8. [PubMed: 17092827]
18. Uskoković V, Wu VM. Calcium Phosphate as a Key Material for Socially Responsible Tissue Engineering. Materials. 2016; 9:434–460. [PubMed: 27347359]
19. Tannoury CA, An HS. Complications with the use of bone morphogenetic protein 2 (BMP-2) in spine surgery. Spine J. 2014; 14:552–559. [PubMed: 24412416]
20. Yang X, Wang YP, Liu FX, Zeng K, Qian MQ, Chen G, Shi L, Zhu GX. Increased invasiveness of osteosarcoma mesenchymal stem cells induced by bone-morphogenetic protein-2. In Vitro Cell Dev Biol Anim. 2013; 49:270–8. [PubMed: 23519562]
21. Eguchi Y, Wakitani S, Imai Y, Naka Y, Hashimoto Y, Nakamura H, Takaoka K. Antitumor necrotic factor agent promotes BMP-2-induced ectopic bone formation. J Bone Miner Metab. 2010; 28:157–64. [PubMed: 19866334]
22. Hustedt JW, Blizzard DJ. The Controversy Surrounding Bone Morphogenetic Proteins in the Spine: A Review of Current Research. Yale J Biol Med. 2014; 87:549–561. [PubMed: 25506287]
23. Shannon RD. Revised effective ionic radii and systematic studies of interatomic distances in halides and chalcogenides. Acta Crystallogr Sect AFound Crystallogr. 1976; 32:751–767.
24. Moroni L, de Wijn JR, van Blitterswijk CA. Integrating novel technologies to fabricate smart scaffolds. J Biomater Sci Polym Ed. 2008; 19:543–572. [PubMed: 18419938]
25. Caminiti, R., et al. Italian Patent No. 01126484-23. 1993.
26. Fosca M, Komlev VS, Yu Fedotov A, Caminiti R, Rau JV. Structural study of octacalcium phosphate bone cement conversion in vitro. ACS Applied Materials and Interfaces. 2012; 4:6202–6210. DOI: 10.1021/am301809y [PubMed: 23088338]
27. Rau JV, Fosca M, Graziani V, Egorov AA, Zobkov Yu V, Yu Fedotov A, Ortenzi M, Caminiti R, Baranchikov AE, Komlev VS. Silver-Doped Calcium Phosphate Bone Cements with Antibacterial Properties. J Funct Biomater. 2016; 7:10.doi: 10.3390/jfb7020010
28. Graziani V, Fosca M, Egorov AA, Zobkov Yu V, Yu Fedotov A, Baranchikov AE, Ortenzi M, Caminiti R, Komlev VS, Rau JV. Zinc-releasing calcium phosphate cements for bone substitute materials. Ceramics International. 2016; 42:17310–17316. DOI: 10.1016/j.ceramint.2016.08.027
29. International Centre for Diffraction Data. Database JCPDS. 2001.
30. Reisner I, Klee WE. Temperature dependence of the ν(OH) bands of hydroxyapatites. Spectrochimica Acta Part A Molecular Spectroscopy. 1982; 38:899–902.

31. Berzina-Cimdina, L., Borodajenko, N. Infrared Spectroscopy - Materials Science, Engineering and Technology, Theophile Theophanides. InTech; Rijeka, Croatia: 2012. Research of Calcium Phosphates Using Fourier Transform Infrared Spectroscopy.
32. Kannan S, Pina S, Ferreira J. Formation of Strontium-Stabilized β-Tricalcium Phosphate from Calcium-Deficient Apatite. J Amer Cer Society. 2006; 89:3277–3280.
33. Barinov SM, Rau JV, Cesaro SN. Carbonate release from carbonated hydroxyapatite in the wide temperature range. J Mater Sci Mater Med. 2006; 17:597–60. [PubMed: 16770543]
34. Ducheyne P, Radin S, King L. The effect of calcium phosphate ceramic composition and structure on in vitro behavior. I. Dissolution. J Biomed Mater Res. 1993; 27:25–34. [PubMed: 8380596]
35. Macomber L, Imlay JA. The iron-sulfur clusters of dehydratases are primary intracellular targets of copper toxicity. Proc Natl Acad Sci U S A. 2009; 106:8344–8349. [PubMed: 19416816]
36. Warnes SL, Caves V, Keevil CW. Mechanism of copper surface toxicity in Escherichia coli O157:H7 and Salmonella involves immediate membrane depolarization followed by slower rate of DNA destruction which differs from that observed for Gram-positive bacteria. Environ Microbiol. 2012; 14:1730–1743. [PubMed: 22176893]
37. Tian WX, Yu S, Ibrahim M, Almonaofy AW, He L, Hui Q, et al. Copper as an antimicrobial agent against opportunistic pathogenic and multidrug resistant Enterobacter bacteria. J Microbiol. 2012; 50:586–593. [PubMed: 22923106]
38. Imlay JA, Chin SM, Linn S. Toxic DNA damage by hydrogen peroxide through the Fenton reaction in vivo and in vitro. Science. 1988; 240:640–642. [PubMed: 2834821]
39. Fatokun AA, Stone TW, Smith RA. Responses of differentiated MC3T3-E1 osteoblast-like cells to reactive oxygen species. Eur J Pharmacol. 2008; 587:35–41. [PubMed: 18448093]
40. Ewald A, Kappel C, Vorndran E, Moseke C, Gelinsky M, Gbureck U. The effect of Cu(II)-loaded brushite scaffolds on growth and activity of osteoblastic cells. J Biomed Mater Res A. 2012; 100:2392–2400. [PubMed: 22528604]
41. Barralet J, Gbureck U, Habibovic P, et al. Angiogenesis in Calcium Phosphate Scaffolds by Inorganic Copper Ion Release. Tissue Eng Part A. 2009; 15:1601–9. [PubMed: 19182977]
42. Gérard C, Bordeleau L-J, Barralet J, et al. The stimulation of angiogenesis and collagen deposition by copper. Biomaterials. 2010; 31:824–31. [PubMed: 19854506]
43. Rodriguez JP, Rios S, Gonzalez M. Modulation of the proliferation and differentiation of human mesenchymal stem cells by copper. J Cell Biochem. 2002; 85:92–100. [PubMed: 11891853]
44. Wu C, Zhou Y, Xu M, Han P, Chen L, Chang J, Xiao Y. Copper-containing mesoporous bioactive glass scaffolds with multifunctional properties of angiogenesis capacity, osteostimulation and antibacterial activity. Biomaterials. 2013; 34:422–33. [PubMed: 23083929]
45. Burghardt I, Lüthen F, Prinz C, Kreikemeyer B, Zietz C, Neumann HG, Rychly J. A dual function of copper in designing regenerative implants. Biomaterials. 2015; 44:36–44. DOI: 10.1016/j.biomaterials.2014.12.022 [PubMed: 25617124]
46. Yang L, Perez-Amodio S, Barrere-de Groot FYF, Everts V, van Blitterswijk CA, Habibovic P. The effects of inorganic additives to calcium phosphate on in vitro behavior of osteoblasts and osteoclasts. Biomaterials. 2010; 31:2976–2989. [PubMed: 20122718]
47. Li S, Wang M, Chen X, Li SF, Li-Ling J, Xie HQ. Inhibition of osteogenic differentiation of mesenchymal stem cells by copper supplementation. Cell Prolif. 2014; 47:81–90. [PubMed: 24450813]
48. Puckett SD, Taylor E, Raimondo T, Webster TJ. The relationship between the nanostructure of titanium surfaces and bacterial attachment. Biomaterials. 2010; 31:706–713. [PubMed: 19879645]
49. Uskokovi V. Nanostructured Platforms for the Sustained and Local Delivery of Antibiotics in the Treatment of Osteomyelitis. Critical Reviews in Therapeutic Drug Carrier Systems. 2015; 32:1–59. [PubMed: 25746204]

Highlights

1. A blue, copper-doped CaP cement with clinically optimal TCP→DCPA setting kinetics.
2. Ca→Cu substitution reduces lattice parameters in all crystallographic directions.
3. The cement is antibacterial, though exclusively against gram-negative bacteria.
4. Simultaneously, the cement increases the viability of a range of human cell lines.
5. More proliferative for primary than cancer cells, suggesting anti-tumorigenicity.

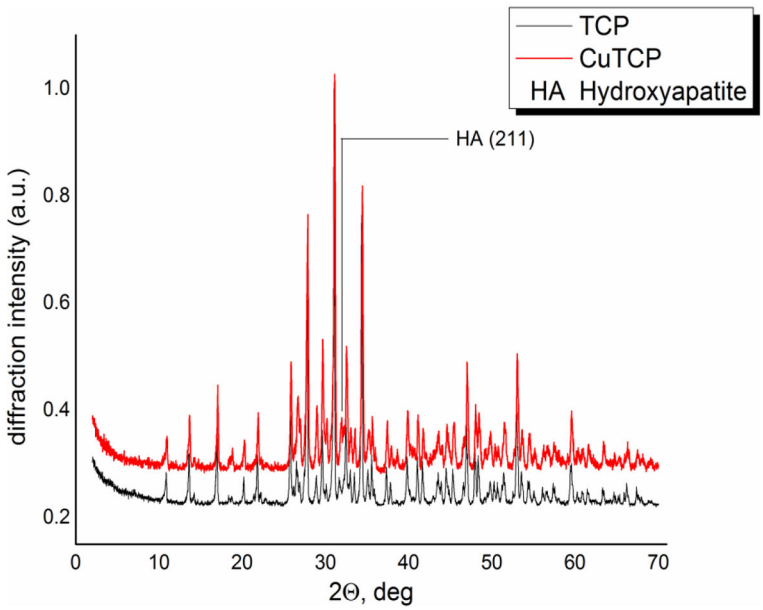

Fig. 1.
XRD patterns of TCP and CuTCP powders after calcination at 900°C.

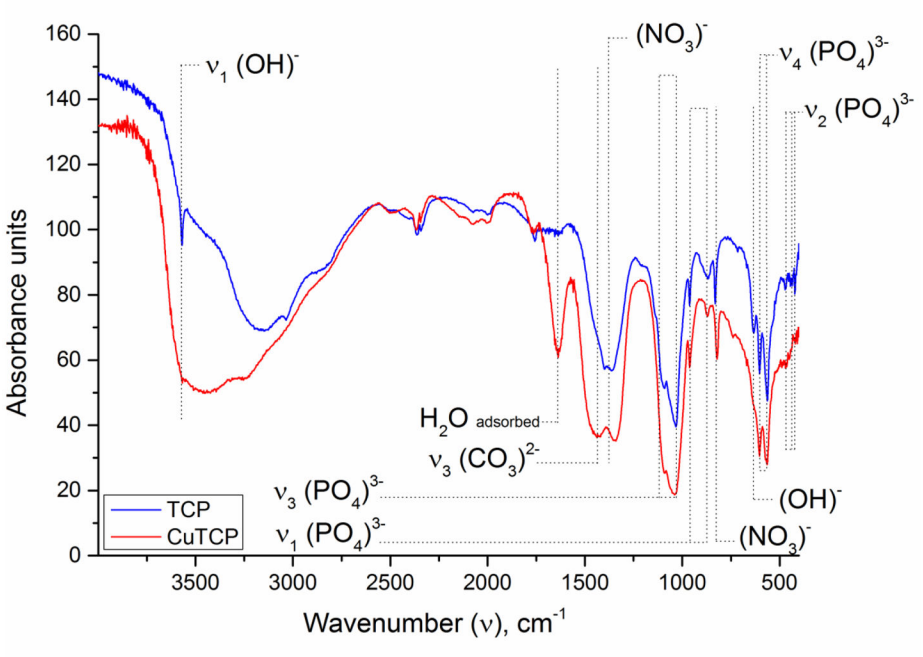

Fig. 2.
IR spectra of pure TCP and CuTCP after annealing at 900°C.

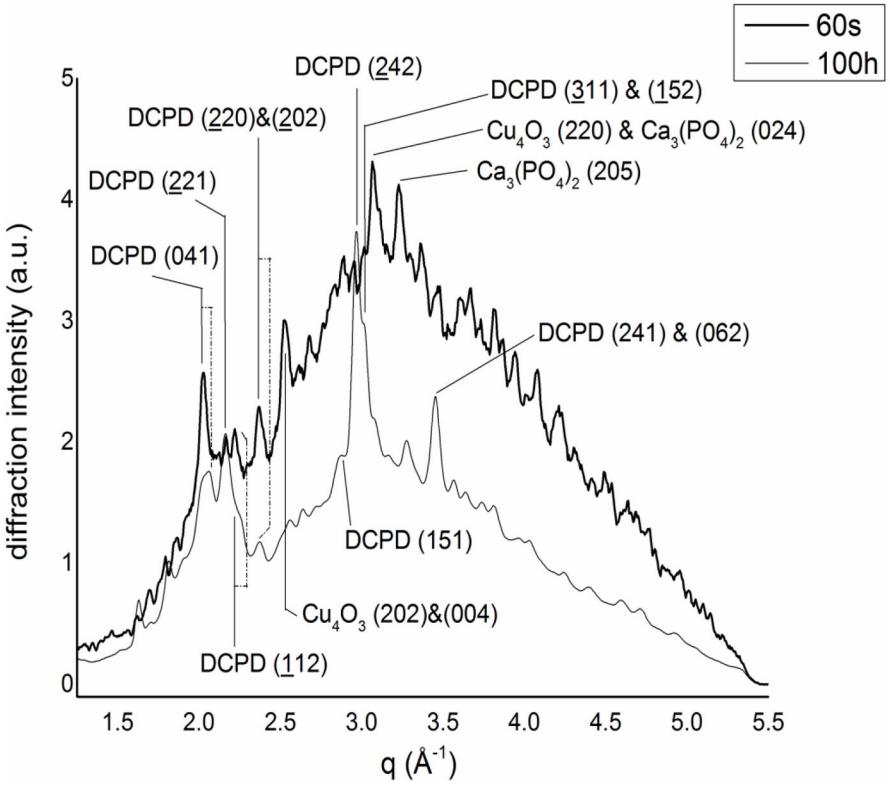

Fig. 3.
Initial (after 60 s) and final (after 100 h) EDXRD spectra of the CuTCP cement.

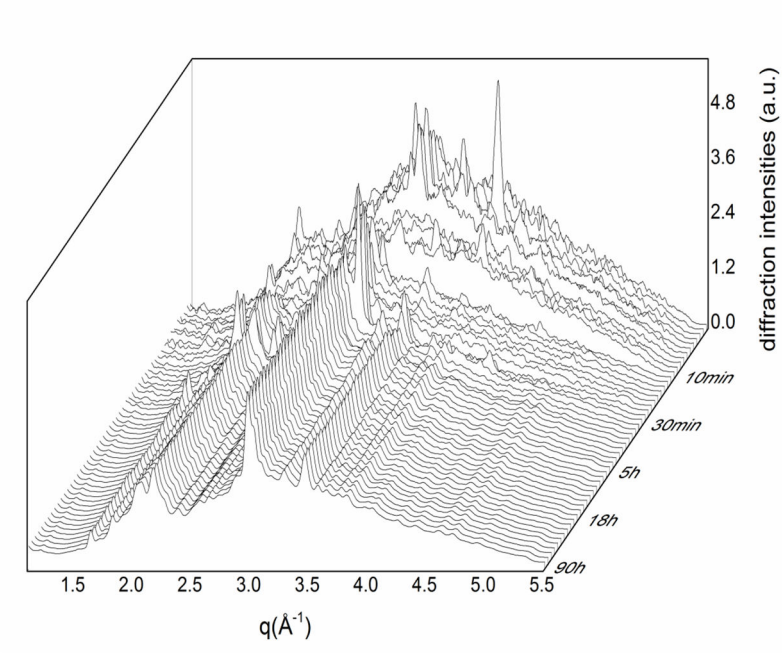

Fig. 4.
3D diffraction map of time evolution of the CuTCP cement hardening process.

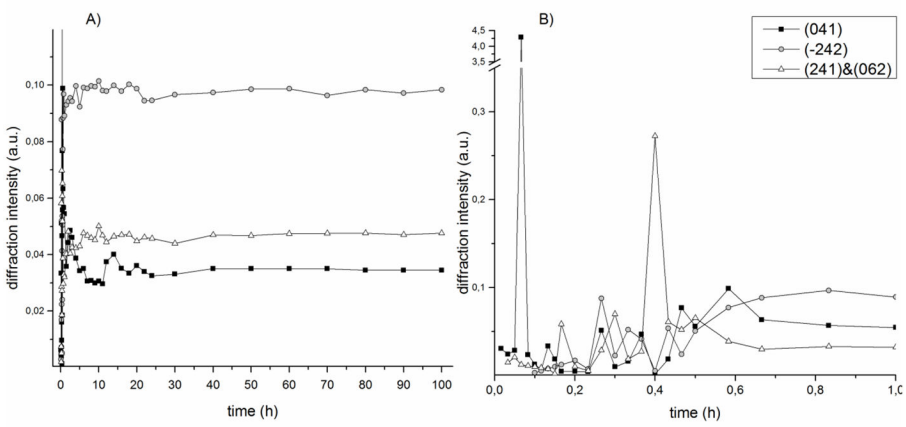

Fig. 5.

Time evolution of the (041), (2̲42) and (241)&(062) brushite peaks: A) overall hardening process; B) first hour of hardening.

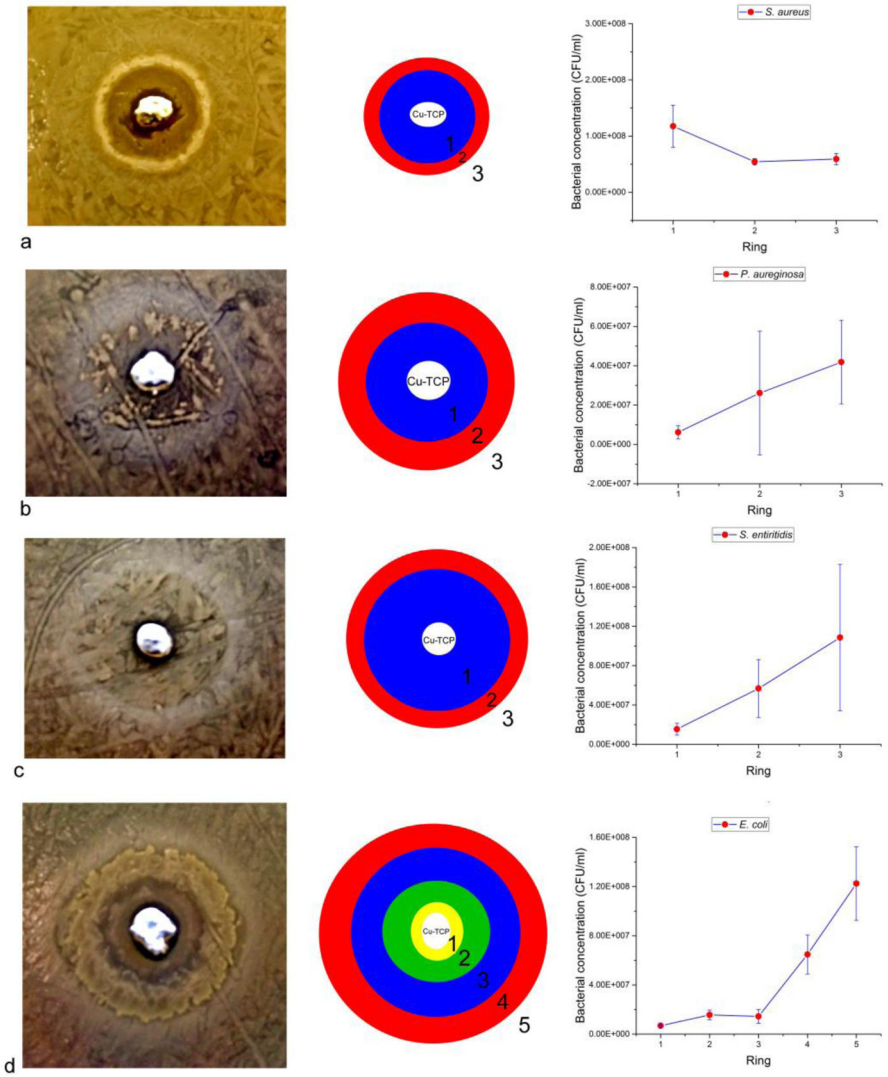

Fig. 6.

Results of the agar diffusion tests of Cu-TCP cements against gram-positive *S. aureus* (a) and gram-negative *P. aeruginosa* (b), *S. enteritidis* (c) and *E. coli* (d). Data points are averages of n=3, while error bars represent standard deviations.

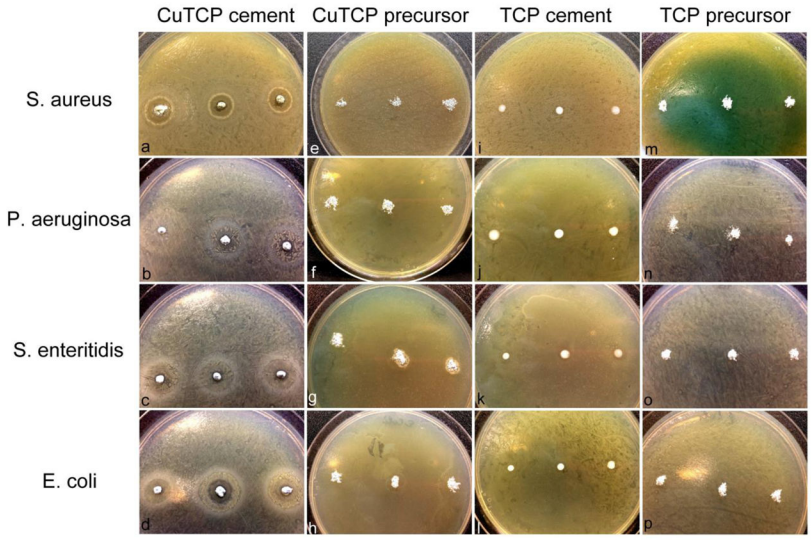

Fig. 7.

Bacterial inhibition zones prominent around the CuTCP cement (a–d) and absent around the precursor CuTCP powder (e–h) and around Cu-free TCP in both the cement form (i–l) and the precursor, powder form (m–p). Assay was carried out against gram-positive *S. aureus* (a, e, i, m) and gram-negative *P. aeruginosa* (b, f, j, n), *S. enteritidis* (c, g, k, o) and *E. coli* (d, h, l, p).

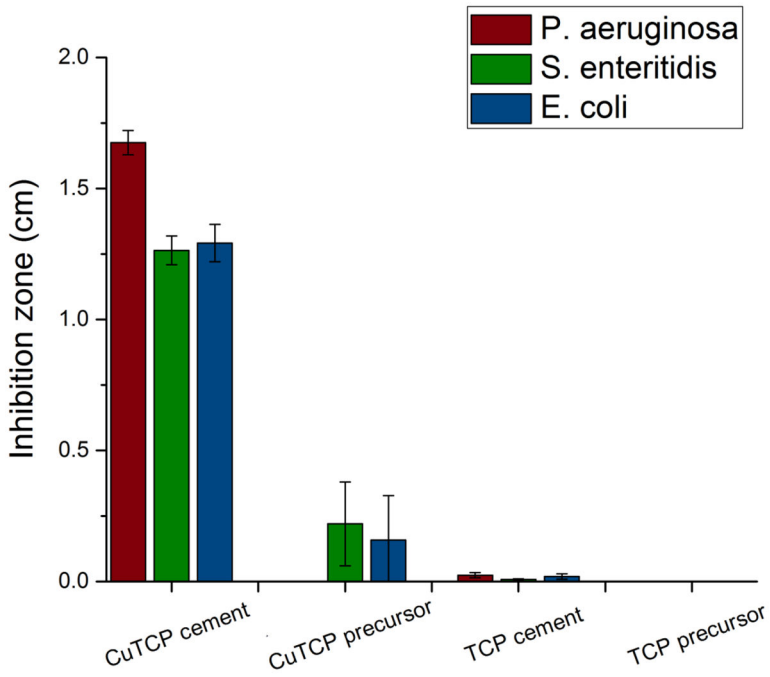

Fig. 8.

The magnitude of inhibition zones around CuTCP and TCP cements and the corresponding precursor powders when tested against three different gram-negative bacteria: *P. aeruginosa*, *S. enteritidis* and *E. coli*.

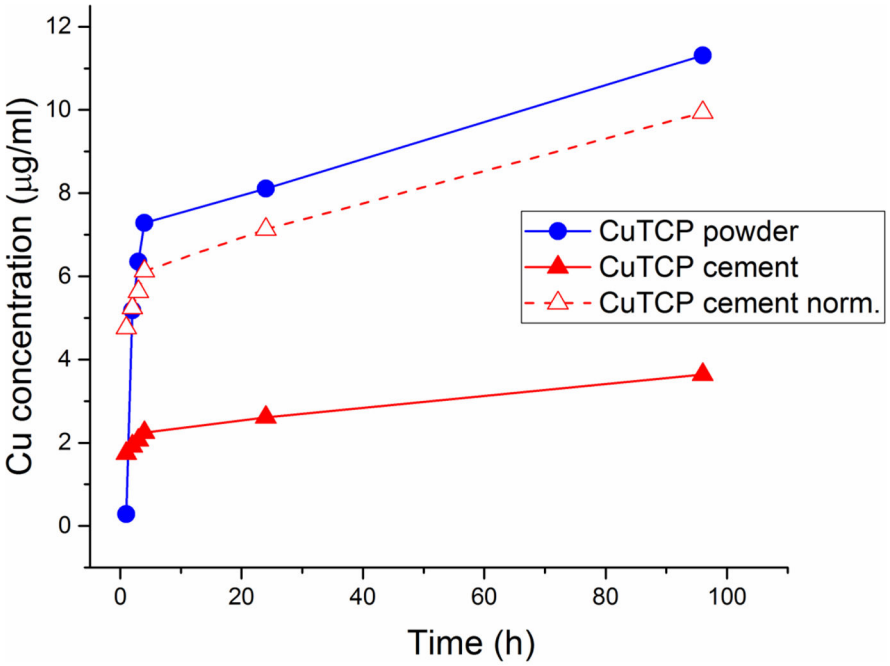

Fig. 9.

Copper ion release from identical amounts of CuTCP powder and CuTCP cement (10 mg/mL) as a function of the immersion time in distilled water. Dashed line represents the copper release from CuTCP normalized to the amount of the copper-releasing CuTCP component of the cement.

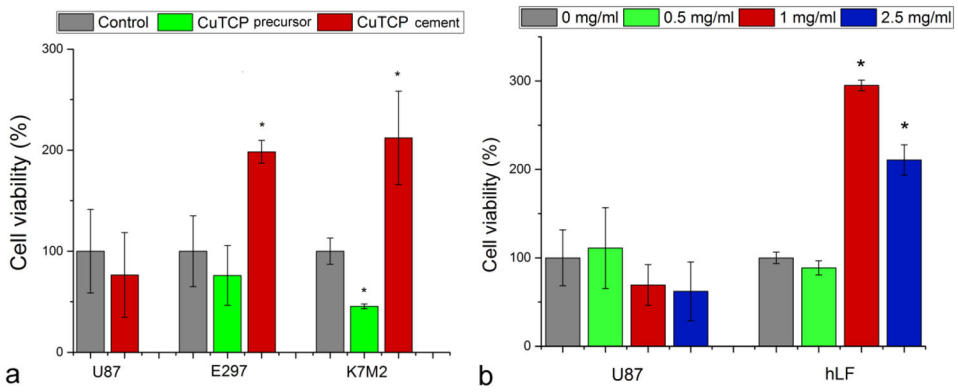

Fig. 10.

(a) Viabilities of U87 and E297 human glioblastoma cells and K7M2 mouse osteosarcoma cells challenged with the precursor CuTCP powder and the hardened CuTCP cement and normalized to the viabilities of the control, untreated cell populations. (b) Dose-dependent viabilities of U87 human glioblastoma cells and human lung fibroblasts (hLF) challenged with the CuTCP precursor powder. Bars and error bars represent means and standard deviations, respectively. The averaged data points statistically significantly higher or lower (p<0.05) compared to the control are marked with an asterisk.

Table 1

Shifts between corresponding diffraction peaks in TCP and CuTCP

Bragg Reflection	$2\theta_{TCP}$ (°)	$2\theta_{CuTCP}$ (°)	$\Delta_{2\theta}$ (°)
(0 1 2)	10.86	10.96	+0.10
(1 0 4)	13.62	13.66	+0.04
(1 1 0)	17.00	17.06	+0.06
(2 0 2)	20.20	20.28	+0.08
(0 2 4)	21.87	21.87	0.00
(1 0 10)	25.78	25.88	+0.10
(2 1 1)	26.52	26.72	+0.20
(2 1 4)	27.78	27.88	+0.10
(3 0 0)	29.61	29.66	+0.05
(0 2 10)	31.02	31.10	+0.08
(1 2 8)	32.44	32.52	+0.08
(2 2 0)	34.34	34.44	+0.10
(1 0 16)	39.80	39.86	+0.06
(4 0 4)	41.06	41.14	+0.08
(3 0 12)	41.66	41.74	+0.08
(4 0 10)	46.94	47.00	+0.06
(2 3 8)	47.94	48.04	+0.10
(4 1 6)	48.34	48.44	+0.10
(2 0 20)	52.98	53.04	+0.06
(5 1 7)	59.54	59.58	+0.04

Table 2

Coherent scattering area values for TCP and CuTCP

Compound	TCP	CuTCP
CSA, nm^2	100±7	84±6

Table 3

Brushite diffraction peak's scattering parameter values.

Bragg peak	q ($Å^{-1}$) theoretical	q ($Å^{-1}$) observed
(041)	2.06	2.03
($\bar{2}$21)	2.15	2.17
($\bar{1}$12)	2.20	2.22
(151)	2.89	2.86
($\bar{2}$42)	2.93	2.96
($\bar{2}$20)&($\bar{2}$02)	2.40	2.37
($\bar{3}$11)&($\bar{1}$52)	3.01	3.01
(241)&(062)	3.45	3.46